Time-Consistent Pressure Relaxation Procedure for Compressible Reduced Navier-Stokes Equations

S. V. Ramakrishnan* and S. G. Rubin†
University of Cincinnati, Cincinnati, Ohio

A time-consistent global pressure relaxation procedure for the unsteady, compressible, reduced Navier-Stokes equations is presented. The shock-capturing capability of the procedure is investigated with different forms of pressure gradient splitting. An efficient conservative method for capturing shocks is detailed. The transient behavior of laminar, high Reynolds number, low subsonic flow past a sine-wave airfoil geometry is analyzed using the new reduced Navier-Stokes-based algorithm. These solutions are compared with steady and unsteady results previously obtained with a modified interacting boundary-layer procedure. The strong influence of grid refinement and the type of differencing of the streamwise convection term on the existence or stability of separated laminar solutions is reaffirmed. More stable turbulent flow results are also presented. Finally, an unsteady solution for the flow past a finite flat plate at incidence is described in order to demonstrate the time accuracy of the algorithm.

I. Introduction

IT is well known that the laminar flow over an airfoil becomes unsteady for sufficiently large Reynolds number and/or angle of incidence. Therefore, it is necessary to consider the time-dependent form of the viscous flow equations in order to study accurately the flow behavior at large Reynolds numbers. In many cases, the full Navier-Stokes (NS) equations can be represented with a reduced form (RNS equations), which can be used to simulate the flow behavior without any significant loss in accuracy. A discussion of the applicability and advantages of the RNS equations can be found in several earlier papers (see, e.g., Refs. 2-4).

In the first part of this paper, the global pressure relaxation procedure for the steady RNS equations developed by Rubin and co-workers has been extended to transient flows. The line relaxation method developed for the steady case[5] has been suitably modified, and the Sherman and Morrison procedure[6] has been incorporated to yield a time-consistent and more stable algorithm. The algorithm has been tested for temporal and spatial consistency in Ref. 7 and is applied here to study the behavior of laminar, large Reynolds number, low subsonic flow past a sine-wave airfoil geometry. This geometry has been examined previously in Ref. 1 with a modified version of interacting boundary-layer (IBL) theory, and some of the results obtained in that study have raised questions of laminar flow stability or breakdown and of the nature of the large Reynolds number flow behavior. The purpose of the present study is to investigate whether the RNS equations provide answers to any of those questions.

The (IBL) results of Rothmayer and Davis[1] may be summarized as follows. For a given thickness ratio ϵ/c of the airfoil, the flow is completely attached for values of Reynolds number R less than a certain value, say $R1$, which is a function of ϵ/c. As R is increased past $R1$, the flow separates downstream of the maximum thickness point, and the length of the separated region increases with R. For values of R larger than $R2$ (ϵ/c), the steady-state IBL model breaks down, i.e., does not converge. Smith showed that this breakdown is manifested through a slow unsteady process that occurs within the separation bubble. The term "unsteady breakdown" has been used in the literature to refer to this behavior. Rothmayer and Davis developed a quasi-steady interacting boundary-layer model to study this unsteady behavior. The temporal behavior of the wall-shear distribution calculated by them was in qualitative agreement with the results of Smith.[8] They conjectured that the unsteady breakdown would eventually lead to massive separation and that the IBL model was inadequate to capture this behavior. They introduced the Sychev-Smith[9] massive separation model in their calculations and obtained solutions with infinite eddies. They encountered a range of values of Reynolds number in which they could obtain multiple solutions, one with a finite and another with an infinite eddy.

The present authors studied the laminar flow past the sine-wave airfoil geometry in order to assess the applicability of the present algorithm and to compare the RNS solutions with the IBL results of Rothmayer and Davis. In particular, a time-consistent, RNS-based algorithm is applied in the range of Reynolds number where the IBL method predicts unsteady breakdown and transition from a finite eddy to an infinite eddy solution. The present investigation concentrates on 1) the development of a time-consistent algorithm for the RNS equations, 2) grid resolution studies to ensure spatial consistency, 3) analysis of temporal accuracy when the breakdown occurs, and finally, 4) comparison with the IBL results.

For the sake of completeness, some turbulent flow solutions are presented in order to demonstrate that with the introduction of a turbulent closure model, it is possible to obtain steady-state solutions at larger Reynolds numbers than those representative of laminar flow breakdown. Finally, unsteady solutions for the flow past a finite flat plate at incidence are also presented to show that the first-order temporal scheme presented here can be used to obtain time-accurate solutions.

In the second part of this paper, solutions for the steady, quasi-one-dimensional flow through a convergent-divergent nozzle with shocks are presented. This study was carried out with a view to establishing the applicability of the algorithm for viscous flows with shocks. Three different forms of pressure gradient splitting have been considered. A novel method of "conservative" pressure gradient splitting, which is applicable for the entire range of Mach number and which captures shocks very efficiently, is discussed in some detail.

Received Dec. 3, 1985; revision submitted Sept. 15, 1986.

*Research Assistant, Department of Aerospace Engineering and Engineering Mechanics.

†Professor and Department Head, Department of Aerospace Engineering and Engineering Mechanics. Associate Fellow AIAA.

Other shock-captured solutions for airfoils and boattail configurations obtained using the technique discussed in this paper have been presented by Khosla and Lai[10] and Reddy and Rubin.[11]

II. Governing Equations

The governing RNS equations in general, orthogonal, curvilinear coordinates are given in Ref. 3. The RNS equations are obtained from the full NS equations by neglecting the second derivative (diffusion) terms in the streamwise direction, as well as all the viscous terms in the normal momentum equation. The energy equation is reduced to a boundary-layer form with Prandtl number equal to unity. The RNS system includes the complete Euler equations and all contributions to IBL theory and triple-deck theory and is therefore more complete than the IBL matching procedure. On the other hand, both the RNS and IBL approximations neglect axial diffusion effects. These terms are generally small for the problems considered here.

Although the algorithm has been developed to solve unsteady, two-dimensional, compressible RNS equations in general, orthogonal, curvilinear coordinates, it suffices, for the purpose of the present discussion, to consider the equations in a sheared Cartesian coordinate system. The equations are written as

Continuity:

$$\rho_t + (\rho u)_\xi - y_b'(x)(\rho u)_\eta + (\rho v)_\eta = 0 \tag{1}$$

X momentum:

$$(\rho u)_t + (\rho u^2)_\xi - y_b'(x)(\rho u^2)_\eta + (\rho uv)_\eta = -[p_\xi - y_b'(x)p_\eta] + (\mu u_\eta)_\eta / R \tag{2}$$

Y momentum:

$$(\rho v)_t + (\rho uv)_\xi - y_b'(x)(\rho uv)_\eta + (\rho v^2)_\eta = -p_\eta \tag{3}$$

Energy:

$$(\rho H)_t + (\rho uH)_\xi - y_b'(x)(\rho uH)_\eta + (\rho vH)_\eta = \frac{(\gamma-1)M_\infty^2}{1+(\gamma-1)M_\infty^2/2} p_t + (\mu H_\eta)_\eta / R \tag{4}$$

Equation of state:

$$\rho T = (1+\gamma)M_\infty^2 p \tag{5}$$

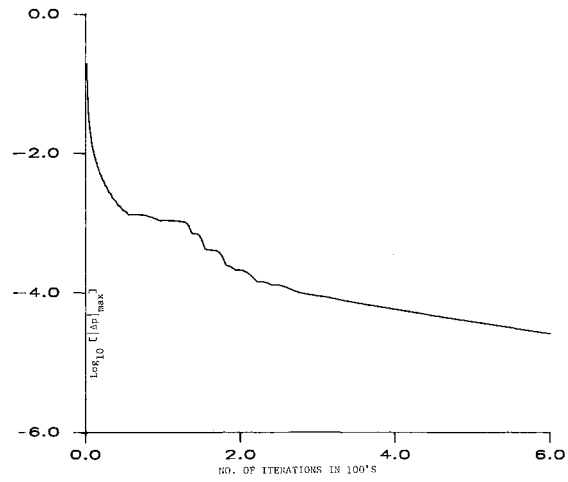

Fig. 1 Convergence rate for the flow over a semi-infinite flat plate; $R = 10^4$, $M_\infty = 0.5$.

where

$$T = [1+(\gamma-1)M_\infty^2/2]H - (\gamma-1)M_\infty^2(u^2+v^2)/2 \tag{6}$$

Viscosity law:

$$\mu = T^\Omega \tag{7}$$

Distances have been normalized with respect to a reference length l^*; the velocities, density, temnperature, total enthalpy, and coefficient of viscosity are normalized with respect to their corresponding freestream values; the pressure $p = (p^* - p_\infty^*)/(\rho_\infty^* u_\infty^{*2})$, the Reynolds number $R = (\rho u l/\mu)_\infty^*$; Ω is a constant. The superscript (*) refers to dimensional quantities. The shearing transformation is given by

$$\xi = x, \quad \eta = y - y_b(x) \tag{8}$$

where $y_b(x)$ describes the body shape.

Boundary conditions:

$\rho(x,y) \to 1, \quad u(x,y) \to u_\infty, \quad v(x,y) \to v_\infty$ as $x \to -\infty$

$\rho(x,y) \to 1, \quad u(x,y) \to u_\infty$ as $y \to \pm\infty$

$u(x,0) = v(x,0) = 0$ on the body

$p_x(x,y) \to 0$ as $x \to \infty$

$H(x,y) \to 1$ as $x \to -\infty$

$H(x,y) \to 1$ as $y \to \pm\infty$ and $H(x,0) = 1$ on the body

For symmetric flows conditions at $y \to -\infty$ are replaced by

$$u_\eta(x,0) = 0, \quad v(x,0) = 0, \quad \text{and} \quad H_\eta(x,0) = 0$$

III. Finite-Difference Algorithm

The difference scheme is developed with the following discrete grid.

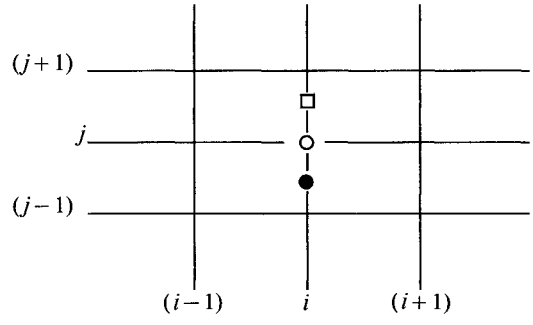

The continuity and y momentum equations (labeled • and □, respectively) are centered at $(i,j-\frac{1}{2})$ and $(i,j+\frac{1}{2})$, respectively and the x momentum and energy equations (labeled ○) are centered at (i,j). First-order backward differencing is used here to approximate the temporal derivatives although second-order accuracy is possible with a slight increase in the memory requirement (see Ref. 7 for further details and solutions). Ghia et al.[12] and Rumsey et al.[13] have previously presented unsteady solutions with first-order time-accurate schemes that agree quite well with experimental data. Hence, for the purpose of the present analysis, the first-order time-accurate version of the algorithm is considered adequate. The effects of temporal step size on the sine wave and a flat-plate geometry are presented to affirm the applicability of a first-order temporal scheme.

The ξ derivatives, except for p_ξ, are generally approximated by a first-order backward-difference formula; although second-order accuracy is achievable with a deferred

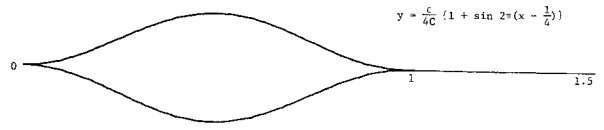

Fig. 2 Sine-wave airfoil geometry.

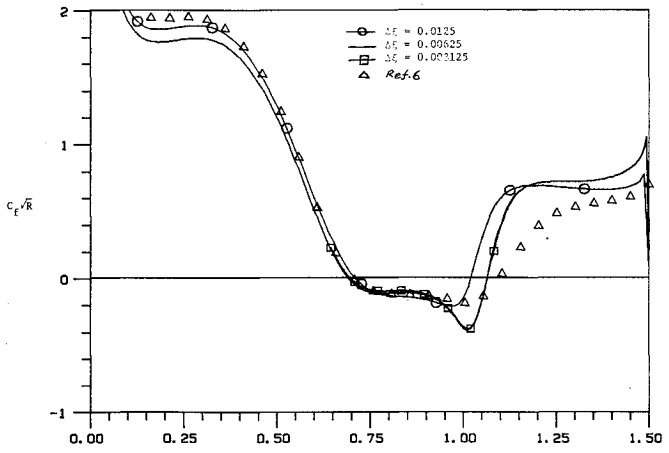

Fig. 3 Wall-shear distribution; $\epsilon/c=0.052$, $R=10^5$.

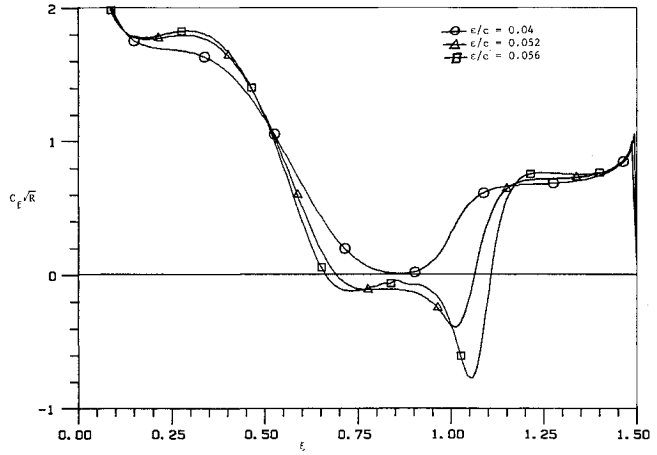

Fig. 4 Effect of thickness ratio on wall-shear distribution; $R=10^5$, $\Delta\xi=0.00625$.

corrector and has been applied for some calculations. In the separated region, the streamwise convection term in the streamwise momentum equation is either completely neglected, resulting in the flare approximation, or is approximated by a first-order upwind difference formula with a second-order deffered corrector. The η derivatives are all approximated by second-order difference formulas. The difference scheme and the global pressure relaxation procedure used here have already been discussed in several earlier papers (see, e.g., Ref. 11 for further details).

For the difference equations, p_ξ is divided into two parts in order to reflect the characteristic domain of the governing RNS system,

$$p_\xi=\omega p_\xi^b+(1-\omega)p_\xi^f \tag{9a}$$

or, in the finite-difference form,

$$(p_\xi)_i=\omega_i(p_i-p_{i-1})/\Delta\xi_i+(1-\omega_i)(p_{i+1}-p_i)/\Delta\xi_{i+1} \tag{9b}$$

where the superscript b refers to a backward-difference or hyperbolic-marching-difference approximation and the superscript f refers to a forward-difference or elliptic-relaxation-difference approximation. The parameter ω is determined by the following relation first given by Vigneron et al.[14] and discussed further in Refs. 2-4

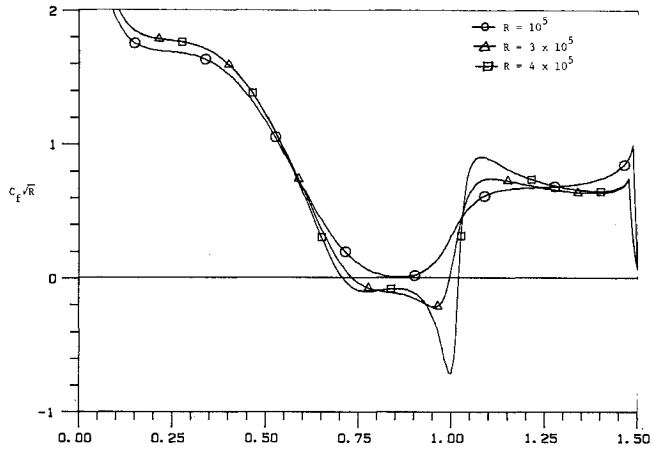

Fig. 5 Effect of Reynolds number on wall-shear distribution; $\epsilon/c=0.04$, $\Delta\xi=0.00625$.

$$\omega=\alpha\gamma M_x^2/[1+(\gamma-1)M_x^2] \quad \text{for } M_x\le 1$$

$$\omega=\alpha \quad \text{for } M_x\ge 1 \tag{10}$$

where $M_x=u^*/a^*$, a^* is the speed of sound and α is a constant such that $0\le\alpha\le 1$.

The resulting nonlinear finite-difference equations are quasi-linearized, such that

$$u(x,y,t)\cdot v(x,y,t)=\bar u(x,y,t)\cdot v(x,y,t)+\bar v(x,y,t)\cdot u(x,y,t)$$
$$-\bar u(x,y,t)\cdot\bar v(x,y,t)$$

where $\bar u$ and $\bar v$ are approximations to u and v. Similar expressions can be obtained for other nonlinear quantities. The above expression is second-order accurate in time when

$$\bar u(x,y,t)=u(x,y,t-\Delta t), \qquad \bar v(x,y,t)=v(x,y,t-\Delta t)$$

The quasi-linearized form of the finite-difference equations, together with the boundary conditions, can be written as

$$A_{i,j}\phi^n_{i-1,j-1}+B_{i,j}\phi^n_{i-1,j}+C_{i,j}\phi^n_{i-1,j+1}+D_{i,j}\phi^n_{i,j-1}+E_{i,j}\phi^n_{i,j}$$
$$+F_{i,j}\phi^n_{i,j+1}+G_{i,j}\phi^n_{i+1,j-1}+H_{i,j}\phi^n_{i+1,j}+I_{i,j}\phi^n_{i+1,j+1}=J_{i,j}$$
$$i=1,2,\ldots M, \quad j=1,2,\ldots N \tag{11}$$

where $\phi=[\rho,u,v]^T$ ($T\rightarrow$transpose) and the superscript n refers to the present time level. The coefficients $A_{i,j}$, $B_{i,j}\ldots,I_{i,j}$ are (3×3) matrices, and $J_{i,j}$ is a (3×1) matrix. All these quantities are functions of $\bar\phi$, which is an approximation to ϕ^n (usually $\bar\phi=\phi^{n-1}$) used in the quasi-linearization of the nonlinear terms and the grid parameters. At every grid point (i,j) except the boundary points, Eq. (11) consists of the continuity equation at $(i,j+\frac{1}{2})$, the y momentum at $(i,j-\frac{1}{2})$, and the x momentum at (i,j). Equation (11) can be written in a concise matrix form as

$$[P+Q]\,V^n=R \tag{12}$$

where the vector V is given by $V=[\rho_{i,j},\ u_{i,j},\ v_{i,j}]^T$ for $i=1,2,\ldots M$ and $j=1,2,\ldots N$. The matrix Q contains the explicit or elliptic terms from the streamwise pressure gradient term and the streamwise convection term in the separated region; P contains all other implicit or marching terms. The

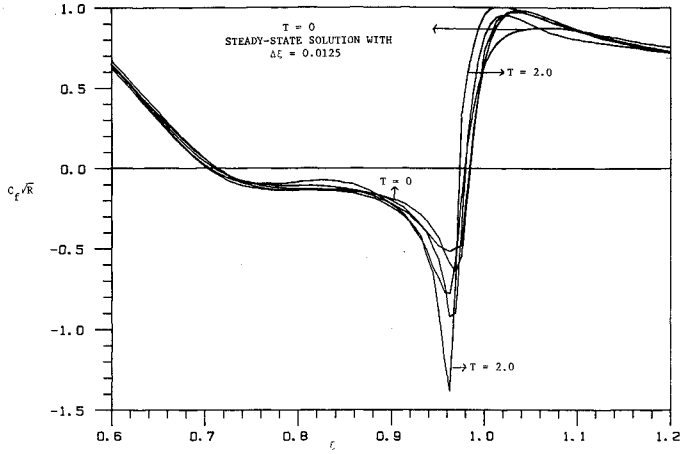

Fig. 6 Transient behavior of wall-shear distribution; $R=6\times10^5$, $\epsilon/c=0.04$, $\Delta\xi=0.00625$.

matrices P and Q are $(M\cdot N)\times(M\cdot N)$ block matrices with (3×3) matrices are elements.

In order to apply the Sherman and Morrison[6] technique to solve Eq. (12), we approximate this equation with

$$[P+Q\bar{V}^n(\bar{V}^n)^T/|\bar{V}^n|^2]\,V^n=R \tag{13}$$

where $\bar{V}^n$ is an approximation to V^n, usually V^{n-1} and the superscript T denotes the transpose. As noted earlier, the matrix Q contains only the terms that result from the forward difference part of the pressure gradient and the $(\rho u^2)_\xi$ term in separated regions. To ensure that Eq. (13) is time-consistent, we write

$$p^n_{i+1,j}=(p^n_{i+1,j}-p^n_{i-1,j})-p^n_{i-1,j}$$

and calculate the elements of the matrix Q from the grouping $(p^n_{i+1,j}-p^n_{i-1,j})$. This method of calculating the elements of Q ensures that Eq. (13) approximates Eq. (12) to first-order accuracy in time when $\bar{V}^n=V^{n-1}$ and hence that Eq. (13) is time-consistent. On the other hand, if the elements of Q were calculated from $p^n_{i+1,j}$, consistency in time would be lost when Eq. (12) is approximated by Eq. (13). This procedure is discussed in detail for both first- and second-order time-dependent and three-dimensional marching procedures in a recent paper by Khosla and Rubin.[7] It has been demonstrated in Ref. 7 that, at least for the model problems considered there, the Sherman and Morrison method does provide a more efficient and stable algorithm.

Equation (13) can be solved exactly (see Appendix) to obtain

$$V^n=P^{-1}L-[P^{-1}Q\bar{V}^n](\bar{V}^n)^TP^{-1}L$$
$$\div\{|\bar{V}^n|^2+(\bar{V}^n)^T[P^{-1}Q\bar{V}^n]\}$$

Since P is a lower diagonal matrix, $P^{-1}L$ and $P^{-1}Q\bar{V}^n$ can be obtained easily using a marching technique.

It should be mentioned here that Eq. (11) does not include the energy equation. The energy equation is uncoupled from the continuity and momentum equations and solved separately with a line relaxation procedure.

The present code is partially vectorized for the CRAY XMP-24 computer. The computational speed of the code is approximately 30 μs/grid point/time step. The convergence rate for the flow over a semi-infinite flat plate with $R=10^4$ and $M_\infty=0.5$ on a 125×41 nonuniform clustered Cartesian grid is shown in Fig. 1. The solution converges to a maximum absolute change in pressure of 10^{-4} in less than 200 iterations. The convergence rate drops considerably after 200 iterations owing to the leading-edge singularity. The algorithm requires less than 600 iterations to achieve four orders of magnitude decrease in maximum absolute change in pressure. In contrast, for this problem, Rumsey et al.[13] require 1500 iterations to achieve the same level of convergence on a 31×120 grid. At this level of convergence, a value of 0.6647 is obtained for the quantity $C_f\cdot(R_x)^{1/2}$. This agrees with the Blasius solution to within 0.1%. With impulsive initial conditions, it is possible to start the computations with a value of the time increment (Δt) such that $\Delta t\le5$. The initial limitation on Δt is due to the discontinuous nature of the impulsive initial conditions. After a few time steps (<50), Δt can be increased to any desired value. This shows that, although the code is developed to solve the unsteady RNS equations, it is very efficient in solving the steady equations as well.

IV. Results and Discussion

The algorithm was initially tested for a finite flat-plate geometry at several Mach numbers. The asymptotic, steady flow solutions were identical to those obtained with the inconsistent form of the algorithm presented in previous studies (see Ref. 5). Further stability studies are also discussed in Ref. 5.

Flow Past a Sine-Wave Geometry

The geometry used in the calculations is shown Fig. 2

$$y_b=\epsilon/4c[1+\sin2\pi(x-\tfrac{1}{4})]\quad\text{for } 0\le x\le1$$

$$y_b=0\quad\text{for } 1<x<1.5$$

Most of the results presented herein are for a freestream Mach number (M_∞) of 0.1 since comparisons with incompressible IBL results are the primary purpose of the present study. All the solutions discussed in this section were obtained using a variable grid in the normal direction containing 50 grid points with a grid spacing of 0.0001 near the body. The wall-shear distribution for a thickness ratio ϵ/c of 0.052 and a Reynolds number R of 10^5 are shown in Fig. 3. Also shown in the same figure is the incompressible wall-shear distribution obtained using interacting boundary-layer theory.[1] It can be seen from this figure that a $\Delta\xi$ of 0.00625 or less is required to calculate the behavior of the separated region accurately. It should be noted here that the solution corresponding to $\Delta\xi=0.003125$ was calculated only in the region $0.5\le\xi\le1.3$; ρ,u and v at $\xi=0.5$ and $\xi=1.3$ were assumed equal to values obtained with $\Delta\xi=0.00625$. The IBL result obtained with a moderate nonuniform mesh is in closer agreement with the present RNS solution for $\Delta\xi=0.0125$.

The effects of ϵ/c and R on the wall-shear distribution are shown in Figs. 4 and 5. It was not possible to obtain a steady-state solution for $\epsilon/c>0.06$ at a Reynolds number of 10^5, or for $R\ge6\times10^5$ for a thickness ratio of 0.04. This is in general agreement with the results of Rothmayer and Davis.[1] The temporal behavior of the wall-shear distribution for $\epsilon/c=0.04$ and $R=6\times10^5$ is shown in Fig. 6. The solution at $t=0$ was obtained by linear interpolation from the converged solution corresponding to $\Delta\xi=0.0125$. The negative peak in the wall-shear distribution increases unboundedly with time and causes the solution to diverge. Similar results were obtained by Rothmayer and Davis[1] for $\epsilon/c=0.04$ and $R=10^6$ (Fig. 7). They applied an unsteady version of the interacting boundary-layer model. A quasi-steady inviscid flow approximation was specified in order to study the unsteady breakdown of the laminar flow calculations. Since the IBL approximations are different from those used in deriving the RNS equations, quantitative agreement between the two theories will not be exact. The fact that the two theories agree qualitatively as to the nature of the "unsteady breakdown" of the laminar flow calculations provides a degree of confidence in the validity of both the procedures.

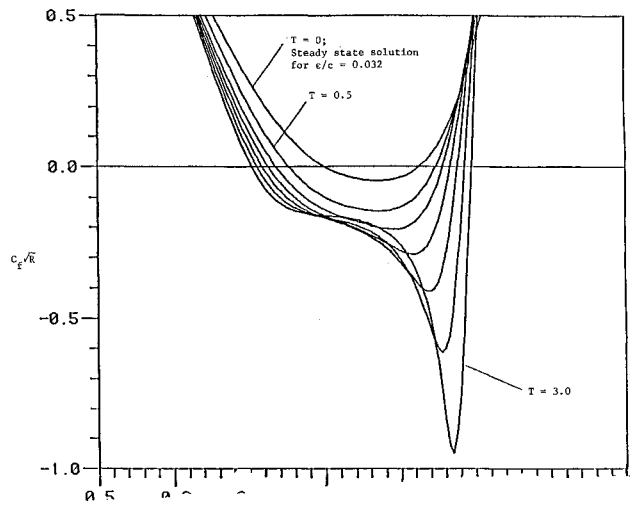

Fig. 7 Transient behavior of wall-shear distribution obtained from IBL theory; $R=10^6$, $\epsilon/c=0.04$.

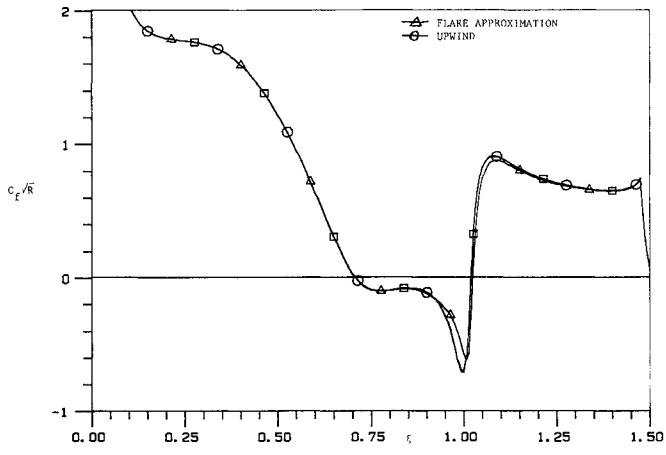

Fig. 8 Effect of flare approximation on the steady-state wall-shear distribution; $\epsilon/c=0.01$, $R=4\times10^5$, $\Delta\xi=0.00625$.

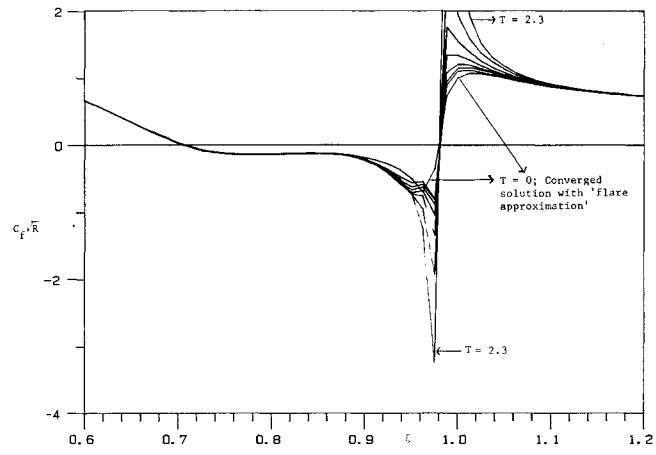

Fig. 9 Transient behavior of wall-shear distribution; $\epsilon/c=0.04$, $R=7\times10^5$, $\Delta\xi=0.0125$.

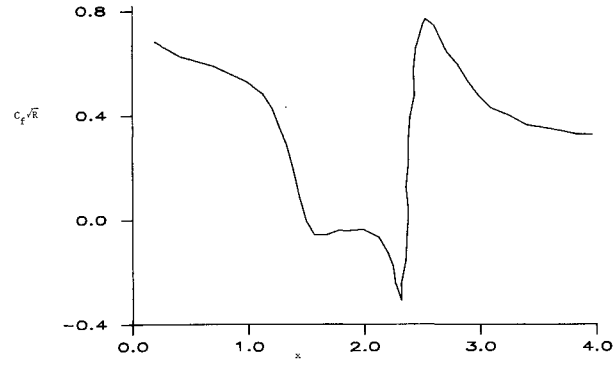

Fig. 10 Steady-state wall-shear distribution for the flow over a trough; $R=4\times10^5$; $M_\infty=0$.

To assert the temporal accuracy of the algorithm, a study of the effect of the temporal step size on the breakdown of laminar solutions for $R=6\times10^5$ was carried out. It was found that, with $\Delta t=5\times10^{-4}$ and 10^{-4}, the breakdown occurred at $t=3.585$ and 3.573, respectively, when the converged solution with $R=5\times10^5$ was used as the initial solution. Every occurrence of breakdown of laminar solutions was veritified with smaller values of Δt to ensure that the breakdown was not indicative of an inherent temporal step size limitation in the algorithm.

Figures 3 and 6 demonstrate the effect of grid resolution on the accuracy of the solution. Significantly, it is possible to obtain steady solutions at larger Reynolds numbers when the grid is relatively coarse. It appears that the coarser grid has a smaller effective Reynolds number or increased numerical viscosity and therefore "stabilizes" the computation. But, even on a coarse grid, the laminar flow solution ultimately fails to converge for sufficiently large values of R. It should be mentioned here that increasing the spatial accuracy of the algorithm with an explicit differed corrector for the axial derivatives was verified to have the same effect as decreasing the grid size.

The effect of the "flare" approximation on the solution is shown in Figs. 8 and 9. From Fig. 8, one can conclude that the flare approximation underpredicts the negative peak in the wall-shear distribution. This is not surprising since, for the case shown in Fig. 8, the negative velocities in the streamwise direction in the recirculation region are not small enough to justify the dropping of the convection terms in that region. It is possible to conjecture from the underprediction of the negative peak in the wall-shear distribution that the flare approximation will have a stabilizing, though possibly erroneous, effect on the calculations. That this is indeed the case can be seen from Fig. 9. Although it is possible to obtain a converged steady-state solution with the flare approximation, the solution diverges with the complete convective model. Both the flare approximation and the coarse grid have two common features: 1) underprediction of the negative peak in the wall-shear distribution and 2) converged steady-state solutions even when such solutions may not exist.

It is appropriate, at this juncture, to say a few words about some results obtained by Edwards and Carter.[15] They were able to obtain a converged solution for $R=4\times10^5$ for the flow over a trough when the flare approximation was applied. They note in their paper that Veldman[16] was unable to obtain convergence for this case when he used a three-point, one-sided difference formula for the convection term in the separated region. The wall-shear distribution, as calculated by Edwards and Carter, is shown in Fig. 10. The wall-shear distribution for the flow over a trough appears similar in certain aspects to that for the flow over a sine-wave airfoil geometry. Therefore, from our experience with the airfoil geometry, one might conclude that Edwards and Carter were able to achieve convergence with $R\geq4\times10^5$ only through the application of the flare approximation in the separated region.

Rothmayer and Davis[1] modeled the transition process from an attached flow to the Sychev-Smith massive separation behavior[7,8] for two-dimensional, thin airfoils at zero

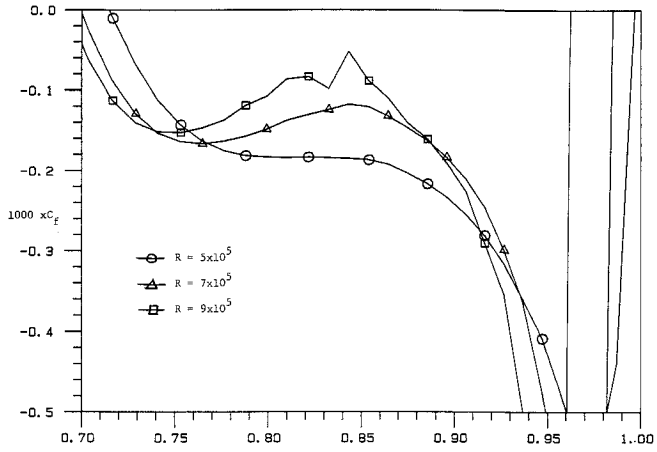

Fig. 11 Effect of Reynolds number on wall-shear distribution in the separated region; $\epsilon/c = 0.04$; $\Delta\xi = 0.0125$.

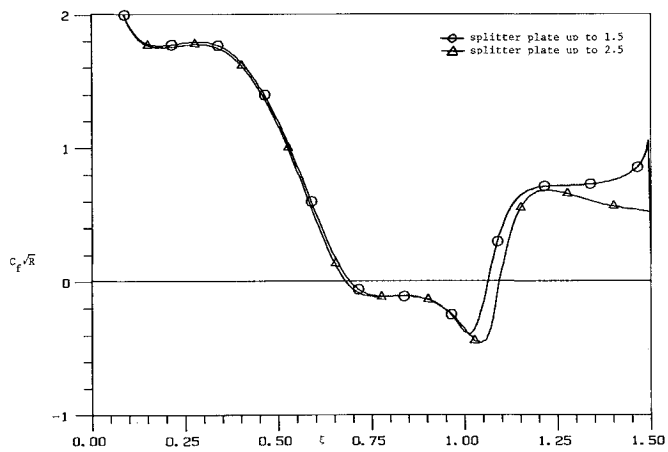

Fig. 12 Effect of splitter plate on wall-shear distribution; $\epsilon/c = 0.052$, $R = 105$, $\Delta\xi = 0.00625$.

angle of attack via the IBL approximation. They obtained a second set of steady-state solutions with this "massive separation" model for some values of ϵ/c and R for which finite eddy solutions had been obtained with the conventional IBL model; i.e., they found that the solution was not unique in some range of values of ϵ/c and R. They also obtained steady solutions with infinite eddies in the range where divergence of the laminar calculations was encountered. In the present study, it has not been possible to obtain solutions exhibiting massive separation from the RNS calculations, nor has a trend toward this behavior been observed as the solution breakdown develops. On the other hand, the wall-shear distribution shown in Fig. 11 seems to indicate that the separation bubble has a tendency to bifurcate into two bubbles as R is increased. It is possible that the solution fails to converge because the grid is not sufficiently fine to resolve this behavior. Further grid refinement studies are required to resolve this question. On the other hand, it should be recalled that moderately fine but coarser grids than are discussed here do lead to stable solutions with a simple recirculation region. It is evident that the physical phenomena may be diffused on the one hand for coarser grids and inadequately resolved or singular on the other hand for fine grids.

It is possible to conjecture other reasons to explain the divergence of the laminar calculations at large Reynolds numbers. On the fine grids, this could be an indication of the onset of turbulence; the present time-consistent calculations, however, may not be able to resolve the transition

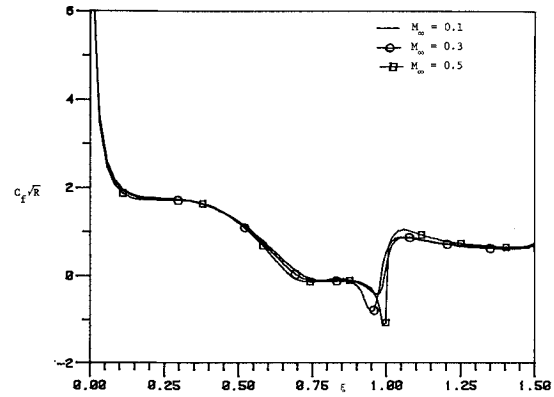

Fig. 13 Effect of Mach number on wall-shear distribution; $\epsilon/c = 0.04$.

behavior accurately. Another possibility is that the imposition of a symmetry condition in the wake region suppresses the bifurcation of the separation bubble into multiple regions of recirculation. The eventual development of quasi-steady multiple vortex patterns or the ultimate shedding of the vortices is therefore suppressed. These could be limiting factors that result in an unsteady breakdown of the calculation. Finally, it might also be conjectured that increasing the length of the splitter plate would prevent shedding and therefore have a stabilizing effect on the calculation. However, it was found that extending the splitter plate up to $\xi = 2.5$, or even $\xi = 3.5$, does not prevent the divergence of the solution or significantly alter the solution. It can be seen from Fig. 12 that increasing the splitter plate does not have a large effect on the solution in the separated region. Therefore, it appears that if it is possible to stabilize the laminar calculations by increasing the length of the splitter plate, this will occur for only a very small range of values of R.

A careful examination of Fig. 9 shows that, except for a region near the reattachment point, the flow tends toward a steady-state solution. Since the wall-shear distribution has large gradients in the vicinity of the reattachment point, one may tend to argue that the unsteady breakdown encountered with both RNS and IBL models may be indicative of the failure of these models under such conditions. But, in a recent study of the same problem with a (linear) direct solver for the stream-function vorticity form of the incompressible NS equations, Bender and Khosla[17] encountered similar behavior, though at a slightly larger Reynolds number. Therefore, the approximations made in RNS and IBL models affect only the value of the Reynolds number at which the unsteady breakdown is encountered, and the unsteady breakdown itself is not the result of the approximations.

For the sake of completeness, the effect of the freestream Mach number (M_∞) on the wall-shear distribution is shown in Fig. 13. The negative peak in the wall-shear distribution increases with M_∞ as does the length of the separated region.

Some turbulent flow calculations were carried out to verify that the introduction of a turbulent closure model will lead to steady-state solutions for the range of values of R and ϵ/c for which the laminar flow calculations exhibit breakdown. The solutions obtained from the turbulent flow calculations confirm this behavior. It has been possible to obtain steady-state solutions for Reynolds numbers up to 5×10^6. Turbulent wall-shear distributions for $\epsilon/c = 0.04$, $R = 10^6$ and $\epsilon/c = 0.16$, $R = 5 \times 10^6$ are shown in Fig. 14. For $\epsilon/c = 0.16$ and $R = 5 \times 10^6$, transition occurs upstream of that corresponding to $\epsilon/c = 0.04$ and $R = 10^6$. The flow is completely attached at the lower Reynolds number and has a small separated region at the larger value of R.

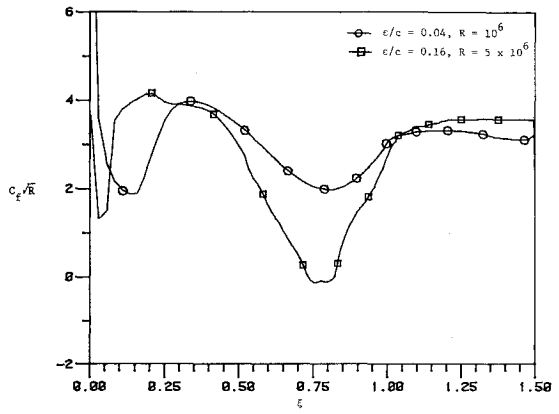

Fig. 14 Turbulent wall-shear distribution.

The turbulent model used here is the Cebeci-Smith[17] eddy-viscosity formulation as modified for a flat-plate near-wake flow by Cebeci et al.[18] To ensure the stability of the calculations, it was necessary to update the eddy viscosity only every few time steps. Since only steady-state turbulent flow calculations have been considered, this has no effect on the accuracy of the solutions. It was found that at larger Reynolds numbers, the eddy viscosity had to be updated less frequently to ensure convergence.

Flow Through a Convergent-Divergent Nozzle with Shocks

The steady inviscid flow through a convergent-divergent nozzle is used as a model problem to study the shock-capturing capabilities of the global relaxation RNS procedure. The effect on the solution of the parameter α in Eq. (10) is shown in Fig. 15. For large values of α, p_x is almost fully hyperbolic, and hence the downstream or back pressure, which determines the shock location, has very little effect on the solution. Therefore, for large values of α, the influence of the downstream pressure does not propagate as far upstream as it should. This results in an incorrect movement of the calculated shock toward the exit as α is increased. Small values of α overestimate the effect of the downstream boundary condition and hence the calculated shock moves too far upstream as α is decreased. Also, the shock is more diffused for smaller values of α.

The results obtained with a local ω form of pressure gradient splitting is shown in Fig. 16. In this case, we write

$$(p_x)_i = \omega_i (p_x^b)_i + (1-\omega_{i+1})(p_x^f)_i \qquad (14)$$

The corresponding finite-difference form of the one-dimensional momentum equation is given by

$$(\bar{p}+\rho u^2)_i - (\bar{p}+\rho u^2)_{i-1} = 0$$

where $\bar{p}_i = (1-\omega_{i+1})\ p_{i+1} + \omega_{i+1} p_i$. The meaning of $\bar{p}$ is discussed in detail in Ref. 11. The above equation shows that the use of Eq. (14) ensures that $(\bar{p}+\rho u^2)$ is conserved everywhere. The results obtained using Eq. (14) indicate that this is a desirable feature. Also, the introduction of ω_{i+1} in the momentum equation at i ensures that the "elliptic" effect of the downstream pressure will propagate upstream, even when $\alpha = 1$. Figure 16 shows that this method of treating the pressure gradient term gives a relatively sharp shock and also predicts the location of the shock wave quite accurately. The convergence history for this case is shown in Fig. 17. The maximum absolute change in pressure decreases by about five orders of magnitude in 460 iterations. Only about 350 iterations are required to achieve 10^{-4} accuracy in pressure. The calculations shown in Figs. 15-17 are for a uniform mesh with $\Delta x = 0.01$ or 200 grid points.

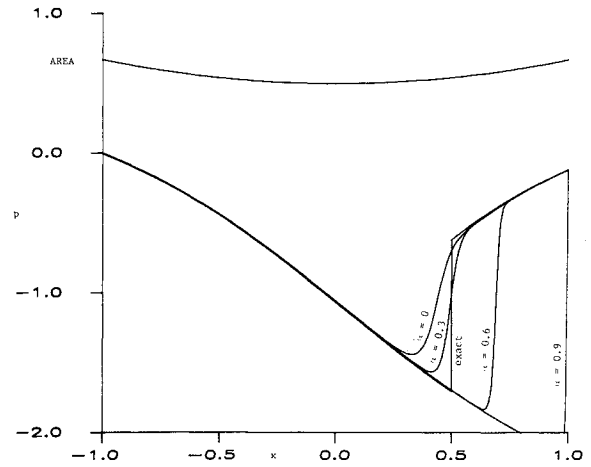

Fig. 15 Effect of α on the pressure solution for a convergent-divergent nozzle.

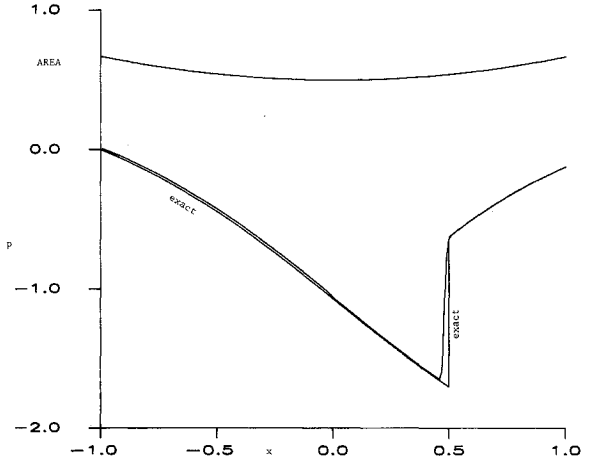

Fig. 16 Pressure distribution obtained using local ω in pressure gradient splitting; $\alpha = 0.99$.

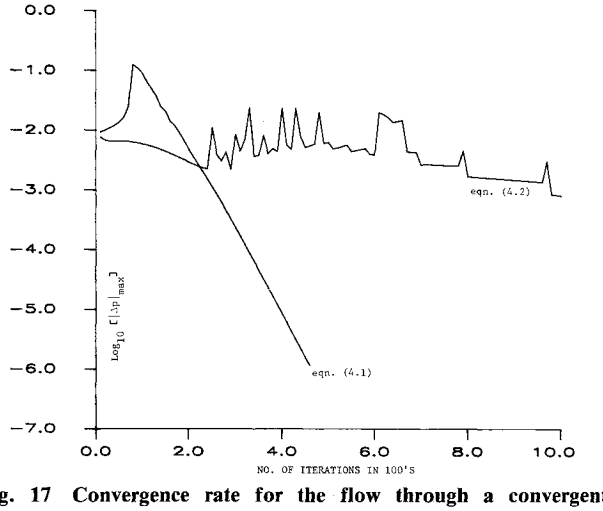

Fig. 17 Convergence rate for the flow through a convergent-divergent nozzle.

It should be pointed out here that it is possible to use $\bar{p}$ as one of the variables instead of p. This would imply that the streamwise pressure gradient is approximated, in all cases, by a backward-difference formula. But, to ensure consistency, it is necessary to split the $(\rho uv)_x$ term in the y-momentum equation (in the case of two-dimensional flows) as

$$(\rho uv)_x \approx \omega_{i+1}(\rho uv)_x^b + (1-\omega_{i+1})(\rho uv)_x^f$$

The appearance of the forward or elliptic difference for ρuv implies that a downstream boundary condition on v is required. In fact, a careful examination of the equations shows that, as before, only a condition on pressure is required at the downstream boundary. This alternative method of treating the elliptic nature of the governing equations through the velocity v does not appear to have any obvious advantages over the global pressure relaxation procedure outlined in this paper and earlier papers by the present authors. However, the analysis does show the close relationship between the p_x term in x momentum equation and the v_x term in y momentum. The elliptic or upstream influence is eliminated if either term is neglected. For hypersonic flows, neglecting the v_x term is termed thin shock-layer theory, and neglecting the p_x term is termed merged layer theory.

In addition to the two methods of p_x differencing discussed so far [Eq. (9) and (14)], a third type of differencing was also considered in order to explore the possibility of further improving the shock-capturing capability of the global RNS relaxation procedure. In this case, we write p_x in a quasi-divergence form as

$$(p_x)_i = \{(\omega p)_x\}_i^b + \{[(1-\omega)p]_x\}_i^f \qquad (15)$$

The flow through a parabolic convergent-divergent nozzle was examined. It was found that the finite-difference equations resulting from Eq. (15) are more sensitive to the value of α than those employing Eqs. (9) or (14); i.e., the solution diverges for $\alpha \geq 0.6$ whereas, in the other two cases, any value of α less than 1 can be prescribed. For $0.45 < \alpha < 0.6$, the solution oscillates. The pressure distribution obtained with $\alpha = 0.45$ is shown in Fig. 18. Since α is small, the shock is more diffused. Also, the pressure distribution has a "kink" in the sonic region. The convergence history for this case is shown in Fig. 17. The oscillations in the maximum absolute change in pressure are caused by both the movement of the shock and by the kink in the pressure distribution in the sonic region. Although Eq. (15) would appear to simulate divergence or conservation differences better, in fact, the quantity $\bar{p} + \rho u^2$ is not properly conserved as it is with Eq. (14).

Taylor series expansions of Eqs. (14) and (15) show that the essential difference between the two forms of differencing arises from the presence of an ω_{xx} term in the truncation error of Eq. (15). Since ω_x is discontinuous at $M=1$ (Fig. 18), $\omega_{xx} \to \infty$ as $M \to 1$, and this results in an increased truncation error and an oscillation in the pressure distribution near $M=1$. The amplitude of the oscillation increases with α and causes the solution to diverge for sufficiently large values of $\alpha < 1$.

A comparison of Figs. 15 and 16 shows that the first type of pressure gradient splitting [Eq. (10)] provides a very good solution in the subsonic region ahead of the throat and that the second type [Eq. (14)] captures the shock efficiently. Note that both types of pressure gradient splitting are identical in the supersonic region. Therefore, it would seem appropriate to employ the first type in the region ahead of the throat and the second type in the region downstream of it. The solution obtained from such a calculation (Fig. 19) shows that this is indeed the best way to treat the pressure gradient term.

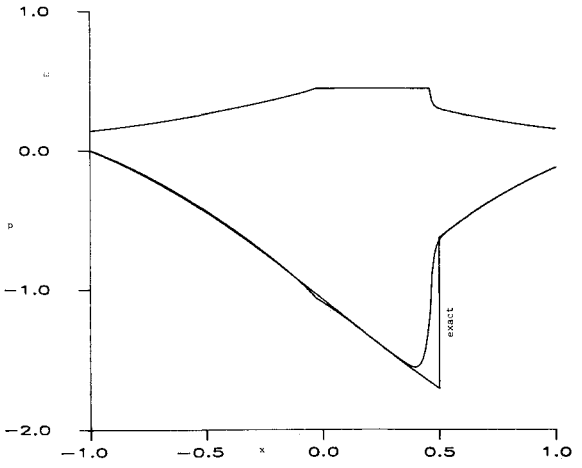

Fig. 18 Pressure distribution obtained using Eq. (15); $\alpha = 0.45$.

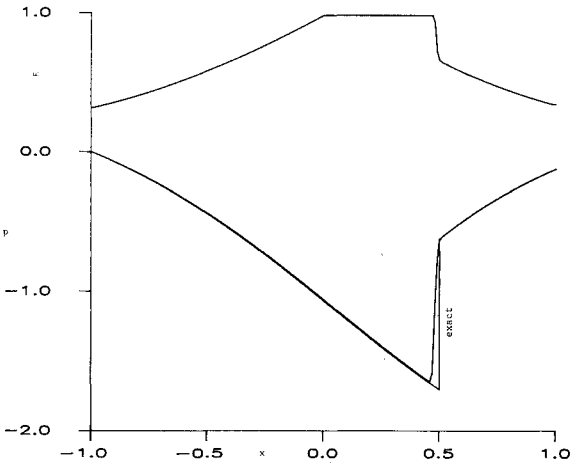

Fig. 19 Pressure distribution obtained using a combination of Eqs. (9) and (14), $\alpha = 0.99$.

Study of the Temporal Accuracy of the Algorithm

Unsteady flow past a finite flat plate at an incidence of 7 deg was used as a model problem for this purpose. The Reynolds number and the Mach number of the sample calculation are 10^4 and 0.3, respectively. The temporal behavior of the lift coefficient calculated with three different values of increment in time ΔT, namely, 0.003, 0.002 and

Table 1 The effect of ΔT on the unsteady solution

ΔT	$(C_L)_{max}$	$(C_L)_{min}$	Strouhal no.
0.0005	0.379	0.313	0.140
0.002	0.377	0.315	0.140
0.003	0.372	0.320	0.140

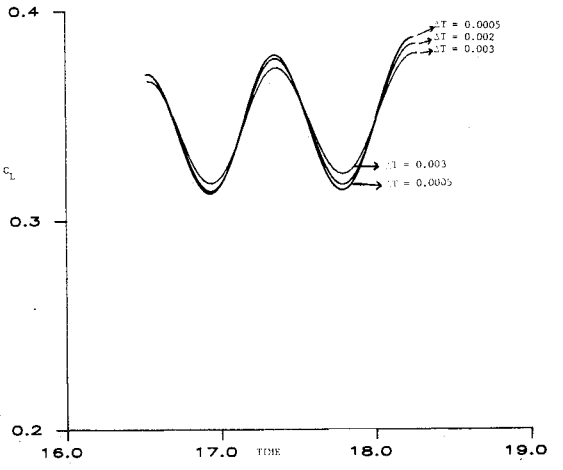

Fig. 20 Transient behavior of the lift coefficient for the flow past a finite flat plate at incidence; $R = 10^4$, $M_\infty = 0.3$, $\alpha = 7$ deg.

0.0005, is shown in Fig. 20. Numerical values for the maximum and minimum values of the lift coefficient and the Strouhal number averaged over two cycles for these values of ΔT are shown in Table 1.

The $(C_L)_{\max}$ and the $(C_L)_{\min}$ values agree to within 2% and the Strouhal number to within 1%. This simple numerical experiment shows that it is indeed possible to obtain reasonably accurate solutions with a first-order time-accurate scheme. One may argue that a second-order time-accurate scheme will provide the same level of accuracy with much larger values of ΔT. But a second-order scheme is likely to have a more severe stability limitation and, thus, the value of ΔT that can be used with a second-order scheme may not be as large as one might expect. More detailed analysis of the RNS solution for the flow past a finite flat plate at incidence will be presented in a forthcoming paper by the authors.

V. Summary

An algorithm to solve the unsteady, compressible RNS equations has been presented. The effect of different types of pressure gradient splitting on the shock-capturing capability of the global RNS procedure has been illustrated. The divergence of laminar calculations found earlier by interacting boundary-layer theory for the flow over a sine-wave airfoil geometry has been studied with the new time-consistent algorithm. It has been shown that up to a point, it is possible to obtain, by using either the flare approximation or a coarse grid, steady-state solutions for values of Reynolds number and thickness ratios at which steady-state solutions do not converge on finite grids or on coarse grids without the flare approximation. For sufficiently fine grids and large enough R or ϵ/c, no steady laminar flow solution could be obtained. This failure may be associated transitional instability or complex vortex or massive separation behavior that has not been adequately resolved. Further study is required. For steady turbulent flow, fully converged solutions have been presented for an arbitrarily large Reynolds number.

Appendix

To solve the matrix equation

$$[P+Qab^T]V=R \tag{A1}$$

where P, Q, and R are $M\times N$ matrices and a, b, and V are $N\times 1$ vectors, premultiply Eq. (A1) by P^{-1}. This yields

$$V+[P^{-1}Qa]b^TV=P^{-1}R \tag{A2}$$

Premultiplying Eq. (A2) by b^T, solving for (b^TV), and substituting back, we get

$$V=P^{-1}R-[P^{-1}Qa][b^TP^{-1}R]/\{1+b^TP^{-1}Qa\}$$

Acknowledgment

This research was supported in part by the Office of Naval Research under Contract N00014-79-C-0849 and in part by the Air Force Office of Scientific Research under Contract F49620-85-C-0027.

References

[1]Rothmayer, A. P. and Davis, R. T., "Massive Separation and Dynamic Stall on a Cusped Trailing Edge Airfoil," *Numerical and Physical Aspects of Aerodynamic Flows*, edited by T. Cebeci, Springer-Verlag, New York, 1985.

[2]Rubin, S. G. and Lin, A., "Marching with the PNS Equations," *Israel Journal of Technology*, Vol. 18, Nos. 1-2, 1980, pp. 21-31.

[3]Rubin, S. G., "Global Relaxation Procedures for a Reduced Form of the Navier-Stokes Equations," *9th ICNMFD*, France, Springer-Verlag, Berlin, June 1984.

[4]Rubin, S. G., "Incompressible Navier-Stokes and Parabolized Navier-Stokes Formulations and Computational Techniques," *Computational Methods in Viscous Flows*, edited by W. G. Habashi, Pineridge, Press, Swansea, Wales, 1984.

[5]Ramakrishnan, S. V. and Rubin, S. G., "Global Pressure Relaxation for Steady, Compressible, Laminar, Two-Dimensional Flows with Full Pressure Coupling and Shock Waves," Department of Aerospace Engineering and Engineering Mechancis, University of Cincinnati, OH, Rept. AFL-84-100, July 1984.

[6]Sherman, J. and Morrison, W. J., "Adjustment of an Inverse Matrix Corresponding to Changes in the Elements of a Given Column or Row of the Original Matrix," *American Mathematical Statistics*, Vol. 20, p. 621.

[7]Khosla, P. K. and Rubin, S. G., "Consistent Strongly Implicit Iterative Procedures," *Journal of Computers and Fluids*, to be published.

[8]Smith, F. T., "Laminar Flow of an Incompressible Fluid Past a Bluff Body: The Separation, Reattachment, Eddy Properties and Drag, Part 2," *Journal of Fluid Mechanics*, Vol. 92, 1979, pp. 171-205.

[9]Sychev, V. V., "On Laminar Separation," *Mechanica Zhidkosti i Gaza*, Vol. 3, 1972.

[10]Khosla, P. K. and Lai, H. T., "Compressible Solutions of the Euler Equations," *Computers and Fluids*, to be published.

[11]Rubin, S. G. and Reddy, D. R., "Analysis of Global Pressure Relaxation for Flows with Strong Pressure Interaction and Separation," *Computers and Fluids*, Vol. 11, No. 4, 1983, pp. 281-306.

[12]Ghia, K., Osswald, G., and Ghia, U., "Analysis of Two-Dimensional Incompressible Flow Past Airfoils Using Unsteady Navier-Stokes Equations," *Proceedings of Third Symposium on Numerical and Physical Aspects of Aerodynamic Flows*, 1985.

[13]Rumsey, C. L., Thomas, J. L., Warren, G. P., and Lui, G. C., "Upwind Navier-Stokes for Separated Periodic Flows," AIAA Paper 86-0247, 1986.

[14]Vigneron, Y. et al., "Calculation of Supersonic Viscous Flow over Delta Wings with Sharp Supersonic Leading Edges," AIAA Paper 78-1137, 1978.

[15]Edwards, D. E. and Carter, J. E., "A Quasi-simultaneous Finite Difference Approach for Strongly Interacting Flow," *Proceedings of Third Symposium on Numerical Physical Aspects of Aerodynamic Flows*, 1985.

[16]Veldman, A.E.P., "A Numerical Method for the Calculation of Laminar Incompressible Boundary Layers with Strong Viscous-Inviscid Interaction," NLR TR 79023 U, 1979.

[17]Bender, E. and Khosla, P. K, private communication.

[18]Cebeci, T. and Smith, A.M.O., *Analysis of Turbulent Boundary Layers*, Academic Press, Orlando, FL, 1974.

[19]Cebeci, T., Thiele, F., William, P. G., and Stewartson, K., "On the Calculation of Symmetric Wakes 1. Two Dimensonal Flows," *Numerical Heat Transfer*, Vol. 2, 1979, pp. 35-60.